Transport in Lattice Fracture Networks: Concentration Mean and Variance

MASSACHUSETTS INSTITUTE
OF TECHNOLOGY
JUL 15 2010
LIBRARIES

by

Peter Kyungchul Kang

Submitted to the Department of Civil and Environmental Engineering
in partial fulfillment of the requirements for the degree of

Master of Science in Civil and Environmental Engineering

at the

ARCHIVES

MASSACHUSETTS INSTITUTE OF TECHNOLOGY

June 2010

© Massachusetts Institute of Technology 2010. All rights reserved.

Author ....
Department of Civil and Environmental Engineering
May 21, 2010

Certified by ....
Ruben Juanes
Assistant Professor of Civil and Environmental Engineering
Thesis Supervisor

Accepted by ....
Daniele Veneziano
Chairman of Departmental Committee for Graduate Students

Transport in Lattice Fracture Networks: Concentration Mean and Variance

by

Peter Kyungchul Kang

Submitted to the Department of Civil and Environmental Engineering
on May 21, 2010, in partial fulfillment of the
requirements for the degree of
Master of Science in Civil and Environmental Engineering

Abstract

We study transport in fractured systems using a stochastic particle tracking approach. We represent a fractured system as a two-dimensional lattice network system where the transport velocity in each fracture is a random variable. Our goal is to develop an exact effective marcroscopic model for the concentration mean and variance from the microscopic disorder model. Within a Lagrangian transport framework, we derive effective equations for particle transport by coarse graining and ensemble averaging of the local scale Langevin equations. The results show that the mean transport can be captured exactly by an uncoupled continuous time random walk (CTRW) and the variance of the concentration by a novel two-particle CTRW formulation. Information about variance of concentration between realizations is important for understanding predictability. Therefore, ensemble mean together with variance provide critical information for understanding and predicting transport through the lattice netowrk.

Thesis Supervisor: Ruben Juanes
Title: Assistant Professor of Civil and Environmental Engineering

Acknowledgments

I appreciate my research advisor Prof. Ruben Juanes for giving me a great opportunity to work with him for my graduate studies. He provided great research opportunities and environment. He helped me to have passion in my research, and always gave great motivation in my research.

I thank Prof. Marco Dentz for his help and guidance. Through his great tutoring and mentoring, I could make this work possible. He is not only a great research mentor but also a great role model in my life.

I thank my family for their enormous love towards me and great support. My dad gave me inspiration to become a researcher and my mom's great support and love always motivate me to become a better person.

I am thankful to all the members of Juanes research group. It is great pleasure that I can continue my PhD work with this wonderful research group.

Last but not the least, I thank all my friends at MIT and outside MIT for fun times that we had and their great support.

Thank you all!

Contents

1 Introduction **11**

1.1 Transport through Network System 12

1.2 Previous Work 13

2 Development of the Analytical Model for the Mean Concentration **17**

2.1 Physical Setting 17

2.2 Methodology 19

2.2.1 Lagrangian Transport Framework 19

2.2.2 Semi-analytical Solution for a Concentration in One Realization 22

2.2.3 Stochastic Modeling and Ensemble Averaging 24

2.2.4 Derivation of the Average Model 24

2.2.5 Eulerian Formulation 32

2.3 Transport Behavior 36

2.3.1 Sensitivity of Mean Concentration with respect to β 37

2.3.2 Evolution of Spreading of the Mean Concentration 39

3 Development of the Analytical Model for the Concentration Variance **41**

3.1 Variability of Concentration 41

3.2 Derivation of the Variance Model 42

3.3 Time Evolution of the Variability 50

4 Conclusions **51**

List of Figures

1-1 Schematic diagram of a dual porosity model. 14

1-2 A 2D example of a discrete fracture network model. 15

2-1 Physical setting of a lattice fracture model. 18

2-2 Concentration field for a fixed realization using particle tracking simulation. 21

2-3 Algorithm for a semi-analytical solution of a concentration in one realization. 23

2-4 Concentration field cuts obtained from the semi-analytical solution and the particle tracking simulations. 23

2-5 Monte Carlo simulation using asynchrnous random walk. 25

2-6 Mean concentration obtained from Monte Carlo simulation. 26

2-7 Mean concentration using Lagrangian CTRW model and Monte Carlo simulation. 31

2-8 Mean concentration using Eulerian CTRW model and Monte Carlo simulation. 36

2-9 One side truncated power law distribution with four different βs. . . . 37

2-10 Mean concentration for four different values of β. 38

2-11 Evolution of spreading for four different values of β. 40

3-1 Concentration variability and variance plot. 42

3-2 Second moment of concentration field obtained from Monte Carlo simulation and two-particle CTRW simulation. 49

3-3 Second moment of concentration field cuts along x-axis. 49

3-4 Time evolution of variability. 50

Chapter 1

Introduction

Networks arise in diverse contexts such as fractured geologic media, transportation infrastructures, social phenomena, and biological systems. Transport trough these network systems has been the focus of much interest. The motivation for this work is to understand flow and transport through fractured porous media. There have been many approaches to predict transport through fractured media. Some models assume that the location and the properties of individual fractures are given. In practice, it is extremely hard to obtain specific properties of fractures and this makes it difficult to apply this type of explicit fracture models to the real world. Traditional models do not generally capture anomalous transport, that is, the nonlinear growth of particle spreading with time. Here, we derive effective equations for particle transport within a Lagrangian transport framework by coarse graining and ensemble averaging of the local Langevin equations that describe motion of individual particle. Our model enables predictions of transport through a lattice network system with limited information. We envision that this first result will lay the foundation for the description of transport in realistic fractured porous media. This approach has the potential to be applied for urban planning, traffic forecasting and the spread of biological and mobile viruses as well.

1.1 Transport through Network System

Understanding flow through fractures is essential for improving several societal related issues, including the risk assessment of nuclear waste disposal [31, 32], the site selection and assessment of leakage risk in geological CO_2 storage [3], the oil and gas production from fractured carbonates [5, 6], and the development of enhanced geothermal systems [2]. Interconnected networks of rock fractures constitute the primary pathways for flow and transport in these applications. However, there are two key obstacles to predicting transport through fractured media. The fundamental challenge is that the location and properties of individual fractures are not identifiable. At best, only some representative properties of the network can be inferred from analogue geologic outcrops or high-resolution seismic interpretation [11, 27]. Second, it is well known that flow through fractures leads to anomalous transport [9, 10, 30]. Anomalous transport refers to the spreading of a substance or a signal in a way that deviates from classical diffusion. Due to these reasons, predictive capabilities of flow and transport in real fractured and heterogeneous media are severely limited.

To model transport through fractured media, we represent fractured porous media as a lattice network system. A network is a set of entities referred as vertices or nodes, with connection between them, called edges or links. The nodes represent the components of a given system, e.g., joints in fractured media; and the links represent existing interactions among nodes, e.g., physical connection, virtual links. Network systems arise in a wide variety of fields, such as the Internet, the World Wide Web, social systems like friendship networks, transportation systems, biological systems like metabolic networks, among many other examples [1, 28]. Therefore, modeling transport through a network system is of interest in many different fields where network system arise.

1.2 Previous Work

Several approaches have been used to model transport through fractured media, including dual porosity models (DPM) [4, 19, 33], discrete fracture networks (DFN) [22, 23, 26], stochastic discrete fracture network [13, 17], and continuous time random walks (CTRW) [7, 8, 9, 10, 25].

In DPM, the rock is modeled as two overlapping continua, one continuum representing the low-permeability matrix and the second continuum representing high-permeability fractures. Because of the dual nature of double-porosity reservoirs, DPM introduces two representative elementary volumes (REV) in describing the system, one for the fracture system and one for the matrix system. The model allows for mass transfer between the matrix system and the fracture system through a transfer function [19]. The fracture system REV is assumed to contain a large number of fractures as shown in Figure 1-1, so that adding or subtracting a few fractures from the REV will not substantially alter its hydraulic properties. The matrix system REV will not be the same as the fracture system REV and will depend upon characteristics of the matrices. In most DPM models, the matrix and fracture system are assumed to be homogeneous and isotropic with regard to their hydraulic properties. Consequently, the REVs will not vary spatially within the reservoir. This is a computationally efficient approach but has limitations. By introducing a REV, the model cannot capture all scales of heterogeneity such as small scale extreme values. Small scale extreme values are critical to accurately model transport. Another shortcoming is the difficulty in accurately evaluating the transfer function between the matrix and fractures [18, 21]. Also, homogeneous and isotropic REV becomes questionable assumption for a fracture system with small number of large-scale fractures, which may dominate the flow. In general, the DPM is an appropriate model for transport in highly and uniformly fractured rock but is inadequate for fracture systems involving moderately or sparsely fractured rock.

In contrast, DFN models represent fractures individually as shown in Figure 1-2. These models can be used for the evaluation of transfer functions for dual-porosity

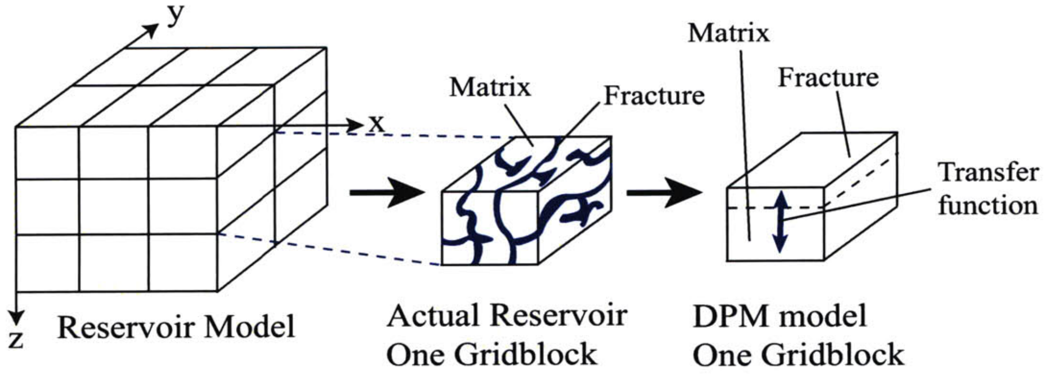

Figure 1-1: Schematic diagram of a dual porosity model showing a typical representative elementary volume (REV) for the densely fractured system.

models, and can also be used in combination with the DPM[20]. DFN is an attractive method because it can consider all levels of heterogeneity by explicitly handing each fracture. In this approach, the small fractures are represented by their effective properties, and the large-scale fractures are modeled explicitly. However, the method requires knowledge of the properties and locations of the individual fractures, which is impossible in practice with current subsurface imaging technology. To overcome this crucial shortcoming, stochastic DFN models have been introduced[13]. In stochastic DFN models, the network geometry is characterized by statistical descriptions of fracture orientation, location, areal extent, and transmissivity. Given this statistical description, multiple realizations of the network are generated, and flow equations are solved to obtain flow characteristics. By repeating this procedure for a large number of realizations, statistics are accumulated on the expected behavior of the system. This approach is computationally intensive, and therefore most applications have been limited to relatively small rock volumes.

Berkowitz and Scher [9, 10] approached the simulation of flow through a fracture network by means of a continuous time random walk (CTRW) — a mathematical description specifically designed to capture anomalous transport by considering all levels of heterogeneity. They generated a number of network realizations using an assumed probability density function of fracture length and fracture angle. Then they solved flow on each network by assuming Darcy flow on each fracture and imposing

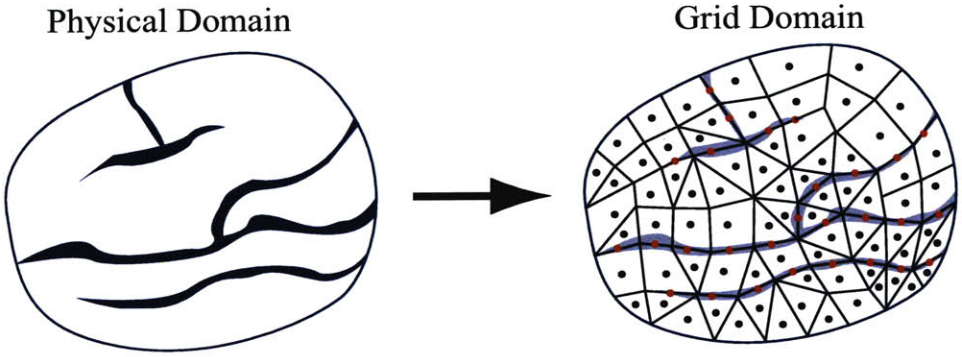

Figure 1-2: A 2D example of a discrete fracture network model. A node is associated with each control volume, and the figure shows that the DFN model can effectively and accurately capture a fracture system with a few major fractures. Modified from Karimi-Fard et al. (2004).

mass conservation at fracture intersections and obtained velocity distribution. The fracture geometry and the velocity distribution are used to map the simulation results onto a joint probability density of the particle jumping distance (corresponding to a fracture length) and the particle transition time (the time spent to travel through a fracture). The procedure to produce the joint probability density function is similar to stochastic DFN, but CTRW uses the joint probability density function for the flow simulation and it has analytical solution for the ensemble mean concentration. Once the joint probability density is known, CTRW is computationally much more effective than stochastic DFN models. This was the first work which successfully applied CTRW framework to capture anomalous flow through fractured media. Their phenomenological approach gave meaningful result and opened new possibility of CTRW on flow through fractured media, but the fundamental theory behind the applicability of CTRW framework onto the fracture network is still unexplained.

Therefore, we propose to develop a stochastic framework for anomalous transport in fractured media which has a firm theoretical background and is computationally efficient. We start with a simple lattice fracture system and show that the ensemble concentration mean and the concentration variance between realizations can be described within the CTRW framework. Recently, a Lagrangian framework was used to upscale unidirectional transport of an adsorbed solute in a chemically heterogeneous medium [15]. In that work, it was shown that the transport through a porous medium with constant hydraulic conductivity and spatially uncorrelated heterogeneous retardation factor follows the CTRW framework. We will generalize the coarse graining and ensemble averaging methodology to the simple 2D fracture network, and develop the effective macroscopic equation from the local scale transport equation. We can systematically prove that the transport statistics through the lattice network system can be effectively captured by CTRW framework. In Chapter 2, we work on mean concentration within Langrangian framework and develop an analytical model for the mean concentration using coarse graining and ensemble averaging. In Chapter 3, we derive governing equation for the concentration variance and show that the variance can also be captured within the CTRW framework. In Chapter 4, we summarize the results and give concluding remarks.

Chapter 2

Development of the Analytical Model for the Mean Concentration

Here, we adopt a Lagrangian viewpoint to develop a macroscopic effective description of transport in a lattice fracture network model. We show that the transport through a lattice fracture network can be described, exactly, as a CTRW that is parameterized by the local scale medium properties and transport characteristics. We will develop an Eulerian formulation by performing a Kramers-Moyal expansion [29] of the Master equation and derive effective equations for the ensemble mean transport. We also work on the moments of the mean concentration and the sensitivity of the plume shape with respect to the local scale medium properties to better understand the transport behavior through the system.

2.1 Physical Setting

We consider a lattice fracture network model consisting of two sets of parallel, equidistant, intersecting fractures: one set at an angle $+\alpha$ and the other at an angle $-\alpha$ with respect to the x-axis, embedded in an impermeable matrix as shown in Figure 2-1. The network is then viewed as a regular lattice of nodes and links. In our fracture model, we assume constant aperture for all links, and a spatially distributed retardation coefficient R for each link. This implies that the flow velocity u through each link of the network is constant, while the effective solute velocity v, which is flow velocity divided by retardation factor $v = \frac{u}{R}$, is spatially variable. In the case of mass transport accompanied by linear sorption, the retardation factor R is defined as $R = 1 + k$, where k is a dimensionless sorption coefficient. The network is random in the sense that the retardation coefficient at each link of the network is drawn from a given statistical distribution. We can think of this procedure as generating a velocity field using limited information. Numerous studies at various scales and in different sites have shown that the distribution of many fracture properties often follows a power law. In nature, the power laws have to be limited by the upper or lower limits to the scale range over which they are valid [11]. Therefore, we assumed a one-sided truncated power law distribution for k, $p_k = N\frac{1}{k^{1+\beta}}\exp(-\frac{1}{k})$, where N is normalization factor and β is a parameter defining the slope of the power law as shown in Figure 2-1. We generate multiple fracture networks realizations using the same p_k for each realization. The set of all realizations generated in this way form a statistical ensemble that is stationary and ergodic. Our goal is to understand transport behavior through this ensemble of network systems.

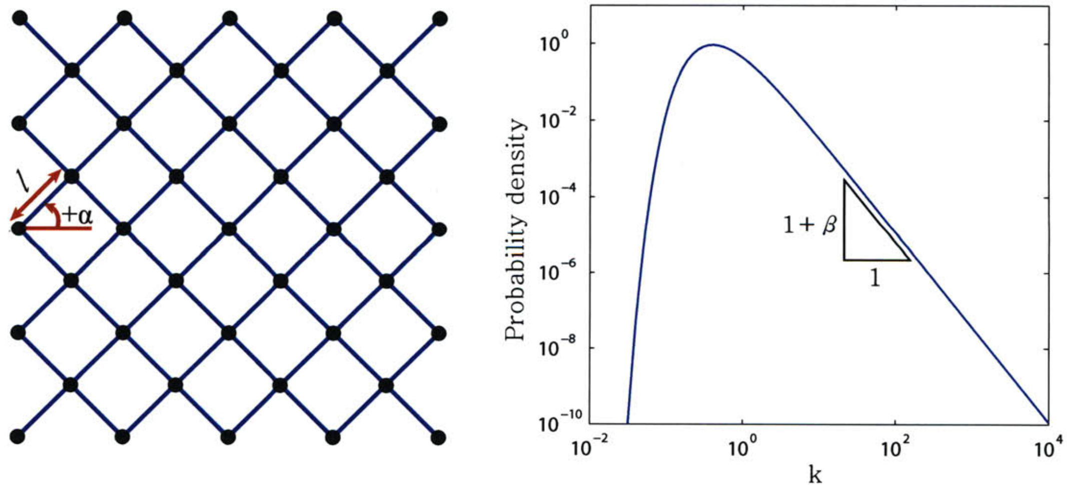

Figure 2-1: A lattice fracture network with the constant fracture length (l) and two sets of fracture orientation $\{-\alpha, +\alpha\}$ with respect to x-axis (left) and the one-sided truncated power law distribution of a dimensionless sorption coefficient (k) with $\beta = 1.5$ (right).

2.2 Methodology

We develop an analytical model for the mean concentration as follows. We first describe the transport through the lattice fracture network using a Lagrangian transport framework. We then perform coarse graining to obtain coarse scale Langevin equation, and perform ensemble averaging to numerically obtain the ensemble mean concentration[15]. The concentration is defined as number of particles at each node divided by the total number of particles and the area represented by the joint. The concentration is equivalent to particle density distribution. For effective model development, we show within the Lagrangian framework that the transport through our network can be exactly described by CTRW framework. Lastly, we develop an Eulerian formulation for the ensemble mean concentration by performing a Kramers-Moyal expansion [29] of the Master equation and solve the equation analytically.

2.2.1 Lagrangian Transport Framework

We first develop a Lagrangian transport framework for transport through the lattice fracture network. This implies solving the local scale equations of motion of particles in a given disorder realization.

Solute transport through our lattice fracture system can be described in terms of Lagrangian equations. Let $\mathbf{x}(t) = [x(t), y(t)]^T$ be the solute particle position at time t. Its evolution with time t is given by

$$\frac{\mathrm{d}x(t)}{\mathrm{d}t} = v[\mathbf{x}(t)] \cos\{\theta[\mathbf{x}(t)]\}, \qquad \frac{\mathrm{d}y(t)}{\mathrm{d}t} = v[\mathbf{x}(t)] \sin\{\theta[\mathbf{x}(t)]\}, \tag{2.1}$$

where $\theta \in \{-\alpha, +\alpha\}$ is the fracture orientation and v is the particle velocity, which varies from fracture to fracture. We rewrite this system of Langevin equations using a time parameterization $t(s)$:

$$\frac{\mathrm{d}x(s)}{\mathrm{d}s} = \cos\{\theta[\mathbf{x}(s)]\}, \qquad \frac{\mathrm{d}y(s)}{\mathrm{d}s} = \sin\{\theta[\mathbf{x}(s)]\}, \tag{2.2a}$$

and

$$\frac{\mathrm{d}t(s)}{\mathrm{d}s} = \frac{1}{v[\mathbf{x}(s)]}, \tag{2.2b}$$

where the random walk $\mathbf{x}(t)$ is parameterized in terms of a continuous variable s, which has a meaning of operational time: the process $s(t)$ is a continuum analog of the number of steps $n(t)$. Through the time parameterization, we can split the time increment and the spatial increment, which enable us to perform coarse graining with the length of the link. The coarse grained equation can be used to perform a space-time asynchronous random walk, which implies that the spatial increment and the time increment are obtained separately.

We develop a coarse-grained Lagrangian formulation of particle motion from Equation (2.2). The spatial transition length is chosen to be of the order of the fracture length because each fracture has constant particle transport velocity. The time increment is determined from the particle transport velocity and the spatial transition length, which makes the time increment spatially variable.

The time evolution of a solute particle takes place on a lattice fracture system with the constant fracture length l and the fracture orientations $\{-\alpha, +\alpha\}$. At each joint, we assume that the particle can enter either of the two fractures with equal probability. This is an appropriate assumption because our fracture network has a constant fracture aperture. Thus, the fine scale Langevin equation (2.2) can be coarse grained by setting $\Delta s = l$, which yields the following discrete equations:

$$x_{n+1} = x_n + l\cos(\alpha), \qquad y_{n+1} = y_n + \xi_n l \sin(\alpha), \tag{2.3a}$$

and

$$t_{n+1} = t_n + \frac{l}{v[\mathbf{x}_n, \xi_n]}, \tag{2.3b}$$

where $\mathbf{x}_n$ is the position of a particle after n jumps, and $\xi_n \in \{-1, +1\}$ represents an equiprobability random process of choosing a fracture $p_{\xi_n} = \frac{1}{2}\delta(\xi_n + 1) + \frac{1}{2}\delta(\xi_n - 1)$, assumed to be independent in time and space, where δ is the Dirac delta function.

To obtain the concentration field of a given realization, we implement this coarse-grained space-time asynchronous random walk, which is orders of magnitude faster than the fine scale synchronous random walk. Transport must still be simulated for many realizations to obtain the concentration statistics because each realization has a different concentration field. We assume a point source at the origin, that is, all the particles are released at $\mathbf{x} = 0, t = 0$. The concentration is defined as the number of particles at each node divided by the total number of particles and the area associated with each joint. Within a realization, the transition time from node to node depends on the position of the particle. The concentration field for a fixed realization using Equation (2.3) is shown in Figure 2-2.

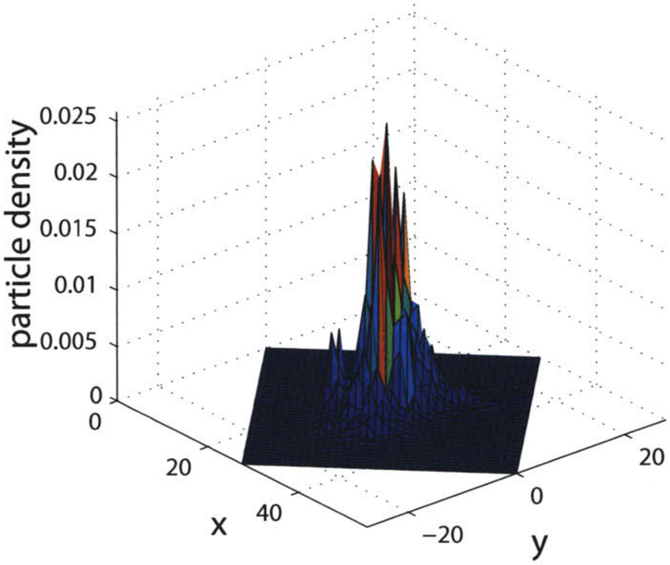

Figure 2-2: Concentration field obtained from particle tracking simulation using Equation (2.3). In this simulation 10,000 particles are injected at $\mathbf{x} = 0, t = 0$ to obtained the concentration field at the fixed target time $t = 50$.

2.2.2 Semi-analytical Solution for a Concentration in One Realization

We solved the transport problem by numerical random walk simulations using Equation (2.3), and obtained a concentration for a given realization. To get an accurate concentration profile for a given realization, we have to inject a large number of particles, which is numerically inefficient. As we increase the number of particles injected, the concentration will converge to the true concentration field. To check the convergence behavior of the particle tracking simulation, we develop an algorithm which calculates the true concentration field.

The key idea is computing all the possible paths for a particle to reach each joint at the target time, and adding up the corresponding probabilities. For each jump, a particle chooses going either up or down with equal probability $\frac{1}{2}$. For a fixed realization, if a particle stays at a joint that needs n jumps to be reached, all the particles taking the same path will stay at the joint at the target time. The corresponding probability for the path which needs n number of jumps, converges to $\left(\frac{1}{2}\right)^n$ as we increase the number of particles injected. To get the full concentration field, we have to consider all the possible paths and add up the probabilities as shown in Figure 2-3.

To verify the algorithm, we compare the concentration field obtained from the developed semi-analytical algorithm with particle tracking simulations. As we increase the number of particles injected, the concentration field converges to the semi-analytical solution which is obtained using the algorithm. By comparing concentration field cuts along $y = 0$, we have verified our algorithm as shown in Figure 2-4. Therefore, we can now generate an accurate concentration field for a fixed realization using the semi-analytical algorithm. This is not only numerically efficient but also gives analytical solution. Especially, when we run Monte Carlo simulations, this makes significant difference in numerical efficiency.

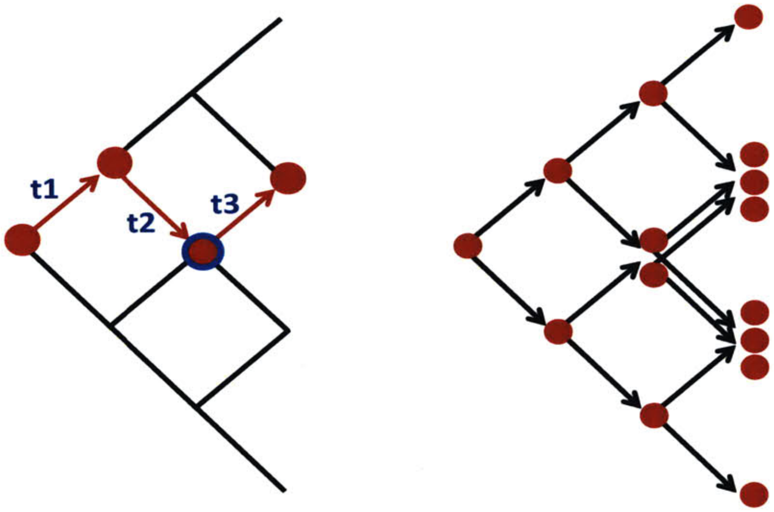

Figure 2-3: If the travel time of a particle following the red arrow $(t1 + t2 + t3)$ is greater than the target time t, all the particles that follow the red path will stay at the second position (red particle with blue outer line), and the probability is $\left(\frac{1}{2}\right)^2$ (left). To get a full concentration field, we have to consider all the possible paths as shown in the figure (right).

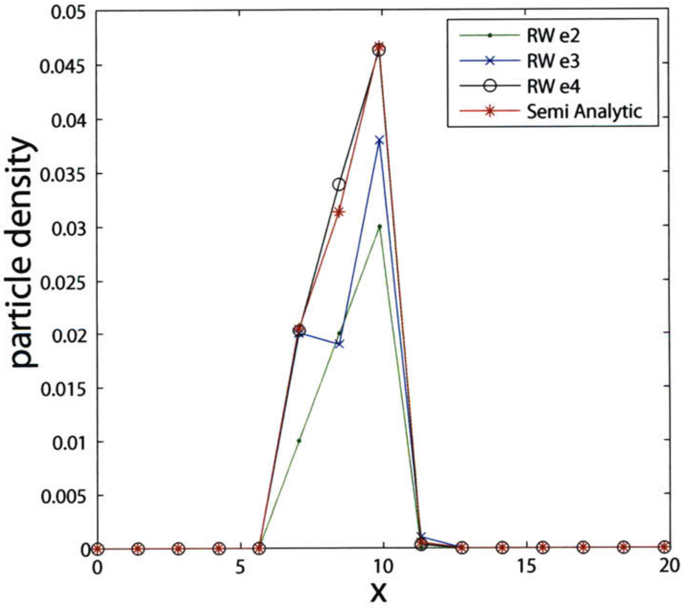

Figure 2-4: Concentration field cuts along $y = 0$ at $t = 30$ for a fixed realization. With increasing number of particles injected, the concentration field converges to the concentration field obtained from the semi-analytical algorithm. With 10^4 particles injected, the concentration field is very close to the semi-analytical solution.

2.2.3 Stochastic Modeling and Ensemble Averaging

So far, we have developed an algorithm to obtain the concentration field for one realization. However, the concentration fields for each realization are all different because each realization has a different velocity field. We simulate transport through different realizations to check the variability between concentration fields. As expected, the result of the simulated concentration fields are highly variable from realization to realization due to differences in the particle velocity field, as can be seen in Figure 2-5. As explained in section 2.1, the velocity fields are generated from a pre-defined one side truncated probability density function. We will follow a Monte Carlo approach, which is simulating transport for a many number of realizations, to obtain representative transport statistics.

We solve the transport problem by numerical random walk simulations using Equation (2.3) for many realizations. We assume a point source at origin as an intial condition. In other words, all the particles are released at $\mathbf{x} = 0, t = 0$. By averaging concentration fields over many realizations, we can obtain a mean concentration field as shown in Figure 2-6. To generate accurate mean concentration field, we simulated transport over 10^4 velocity fields, which is numerically very expensive. Our goal is to develop an effective model for a mean concentration in a systematic way. We work on the variability of concetration fields between realizations in Chapter 3.

2.2.4 Derivation of the Average Model

In this section, we develop an effective model for the mean concentration which we call the average model. Our goal is to derive a Lagrangian system of equations for the effective mean particle movements. In order to obtain the average particle motion, the single particle density will be averaged over the noise which models diffusion and over the configurational disorder [14, 15]. This will lead to an effective Lagrangian formulation of mean particle movements, which maps the disorder statistics of the random network into random increments in the particles' equations of motion. The developed effective Langevin equations for the particle motion in space-time will represent the

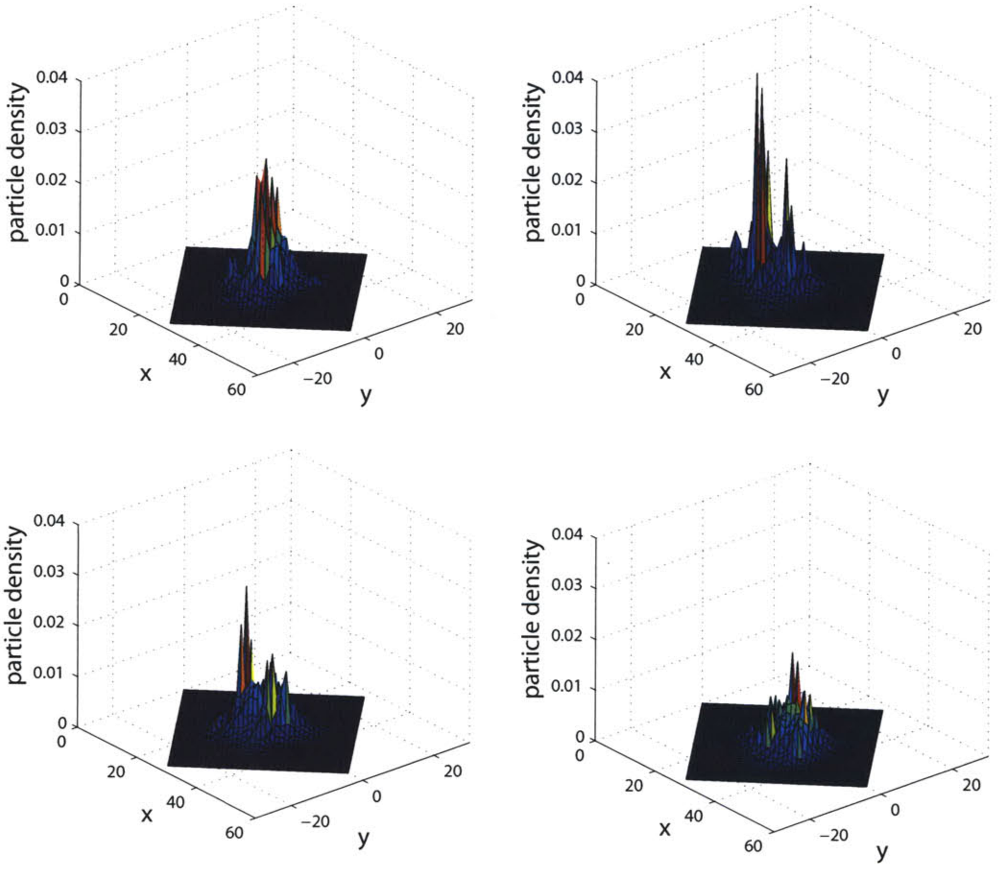

Figure 2-5: Concentration fields obtained by numerical random work simulations over four different velocity fields at $t = 50$. Each velocity field is generated from the same probability density distribution and the result shows the large variability between concentration fields.

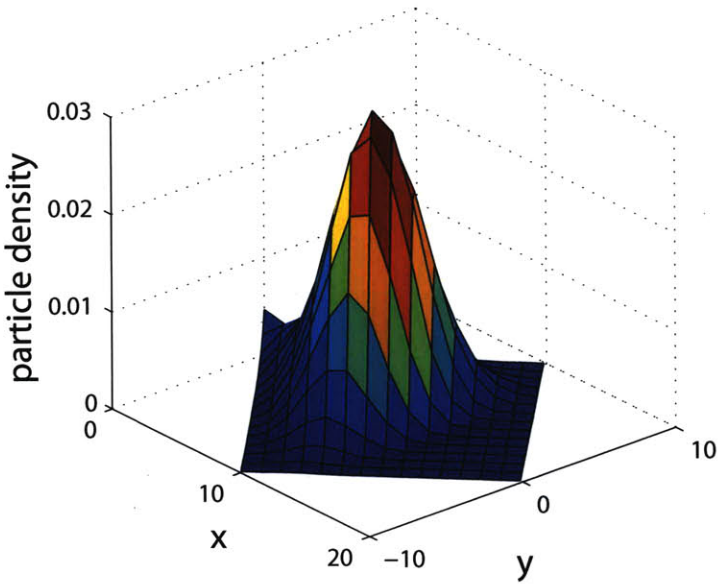

Figure 2-6: Mean concentration field at $t = 30$ obtained by averaging over 10^4 concentration fields from Monte Carlo simulation. Each velocity field was generated from the one side truncated probability density distribution, and each velocity field is stationary and ergodic.

ensemble mean transport behavior.

The particle distribution $c(\mathbf{x}, t)$ in a single realization is given by

$$c(\mathbf{x}, t) = \langle \delta \left\{ \mathbf{x} - \mathbf{x}[s(t)] \right\} \rangle, \tag{2.4}$$

where δ denotes the Dirac delta distribution, and the angular brackets denote white-noise average over many solute particles. The ensemble average of the particle distribution over realizations (i.e., the ensemble mean concentration) is given by

$$\overline{c(\mathbf{x}, t)} = \overline{\langle \delta \left\{ \mathbf{x} - \mathbf{x}[s(t)] \right\} \rangle}, \tag{2.5}$$

where the overbar denotes the ensemble average over realizations. Using the property of the delta function, we can rewrite Equation (2.5) as,

$$\overline{c(\mathbf{x}, t)} = \int ds \overline{\langle \delta(\mathbf{x} - \mathbf{x}(s)) \delta(s - s(t)) \rangle}, \tag{2.6}$$

If we perform the ensemble averaging prior to the noise averaging,

$$\overline{c(\mathbf{x},t)} = \int ds \left\langle \overline{\delta(\mathbf{x}-\mathbf{x}(s))\delta(s-s(t))} \right\rangle \tag{2.7}$$

By performing the ensemble averaging first, we can use the stationarity of the velocity field. If we assume point injection as an initial condition, the probability of a particle being at a certain position after a fixed number of jumps is same for all realizations because the topology of the fracture network is fixed, and we assumed equal probability of jumping upward and downward at each joint. Thus, when we perform the configuration average, we only need to average over $\delta(s - s(t))$, and we can write Equation (2.7) as,

$$\overline{c(\mathbf{x},t)} = \int ds \langle \delta(\mathbf{x}-\mathbf{x}(s)) \overline{\delta(s-s(t))} \rangle \tag{2.8}$$

By coarse-graining Equation (2.8) with the length of a link (l),

$$\overline{c(\mathbf{x},t)} = \sum_{N=0}^{\infty} \langle \delta(\mathbf{x}-\mathbf{x}_N) \overline{\delta_{N,N_t}} \rangle \tag{2.9}$$

Where $\mathbf{x}_N$ is the position of a particle after N jumps, and N_t is the number of jumps during time t. Note that $\overline{\delta_{N,N_t}}$ is the probability that after N steps the time t is between t_N and t_{N+1}. Therefore, we can rewrite $\overline{\delta_{N,N_t}}$ using indicator function (I) as,

$$\begin{aligned} \overline{\delta_{N,N_t}} &= \overline{I(t_N \leq t < t_{N+1})} \\ &= \overline{I\left(0 \leq t - t_N < \frac{l}{v_N}\right)} \\ &= \overline{\int dt' \delta(t'-t_N) I\left(0 \leq t - t' < \frac{l}{v_N}\right)} \end{aligned} \tag{2.10}$$

Since t_N and v_N are independent from Equation (2.3),

$$\overline{\delta_{N,N_t}} = \int dt' \overline{\delta(t'-t_N)}\, \overline{I\left(0 \leq t - t' < \frac{l}{v_N}\right)} \tag{2.11}$$

Since the velocity fields are generated from a probability density function $P(v)$ which can be derived from a predefined one side truncated probability density function of the retardation factor p_k, the velocity fields are statistically stationary. Therefore, we can write $\overline{I\left(0 \leq t - t' < \frac{l}{v_N}\right)}$ as,

$$\overline{I\left(0 \leq t - t' < \frac{l}{v_N}\right)} = \int_0^\infty dvP(v)I\left(0 \leq t - t' < \frac{l}{v}\right) \tag{2.12}$$

If we say $\psi(\tau)$ is a probability density function of a particle jumping time, we can derive $\psi(\tau)$ from $P(v)$ using the relationship $\tau = \frac{l}{v}$ and the fact that l is a constant as following.

$$v = \frac{l}{\tau} \rightarrow dv = -\frac{l}{\tau^2}d\tau \tag{2.13}$$

$$\begin{aligned} \psi(\tau') &= \int_0^\infty dvP(v)\delta(\tau' - \frac{l}{v}) \\ &= \int_\infty^0 -\frac{l}{\tau^2}d\tau P(\frac{l}{\tau})\delta(\tau' - \tau) \\ &= \frac{l}{\tau'^2}P(\frac{l}{\tau'}) \end{aligned} \tag{2.14}$$

Therefore, we can rewrite Equation (2.12) using $\psi(\tau)$ as,

$$\begin{aligned} \overline{I\left(0 \leq t - t' < \frac{l}{v_N}\right)} &= \int_0^\infty d\tau\psi(\tau)I\left(0 \leq t - t' < \tau\right) \\ &= \int_{t-t'}^\infty d\tau\psi(\tau) \end{aligned} \tag{2.15}$$

From Equation (2.11) and Equation (2.15),

$$\overline{\delta_{N,N_t}} = \int_0^t dt'\overline{\delta(t' - t_N)}\int_{t-t'}^\infty d\tau\psi(\tau) \tag{2.16}$$

From Equation (2.9) and Equation (2.16), the ensemble concentration can be written as,

$$\begin{aligned}\overline{c(\mathbf{x},t)} &= \int_0^t dt' \sum_{N=0}^{\infty} \langle \delta(\mathbf{x}-\mathbf{x}_N)\overline{\delta(t'-t_N)}\rangle \int_{t-t'}^{\infty} d\tau\psi(\tau) \\ &= \int_0^t dt' R(\mathbf{x},t')\left[1-\int_0^{t-t'} d\tau\psi(\tau)\right] \qquad (2.17)\end{aligned}$$

Where $R(\mathbf{x},t')$ is defined as,

$$\begin{aligned}R(\mathbf{x},t') &= \sum_{N=0}^{\infty} \langle \delta(\mathbf{x}-\mathbf{x}_N)\overline{\delta(t'-t_N)}\rangle \\ &= \sum_{N=0}^{\infty} P_N(\mathbf{x},t) \qquad (2.18)\end{aligned}$$

Using Chapman-Kolmogorov equation, we express P_N with a transition probability and P_{N-1}.

$$\begin{aligned}P_N(\mathbf{x},t) &= \langle \delta(\mathbf{x}-\mathbf{x}_N)\overline{\delta(t-t_N)}\rangle \\ &= \int d\mathbf{x}' \int dt' \left\langle \delta((\mathbf{x}-\mathbf{x}')-\Delta\mathbf{x})\overline{\delta((t-t')-\Delta t)}\right\rangle P_{N-1}(\mathbf{x}',t') \qquad (2.19)\end{aligned}$$

Now the only term with ensemble averaging is the time transition probability. Using the fact that a velocity at each fracture is independent of spatial position and statistically ergodic after ensemble averaging,

$$\begin{aligned}\overline{\delta((t-t')-\Delta t)} &= \overline{\delta\left((t-t')-\frac{l}{v(\mathbf{x}_{N-1})}\right)} \\ &= \int_0^{\infty} dv P(v)\delta\left((t-t')-\frac{l}{v}\right) \\ &= \int_0^{\infty} dv P(v)\frac{v}{t-t'}\delta\left(v-\frac{l}{t-t'}\right) \\ &= P\left(\frac{l}{t-t'}\right)\frac{l}{(t-t')^2} \equiv \psi(t-t') \qquad (2.20)\end{aligned}$$

Equation (2.20) implies that in configuration average, the time increment is independent of spatial position and of the spatial increment as long as the underlying random field is statistically stationary. From Equation (2.20), we can rewrite the transition probability as,

$$\left\langle \delta((\mathbf{x}-\mathbf{x}')-\Delta\mathbf{x})\overline{\delta((t-t')+\Delta t)}\right\rangle = \langle \delta((\mathbf{x}-\mathbf{x}')-\Delta\mathbf{x})\rangle\, \psi(t-t') \tag{2.21}$$

Now let's work on the spatial transition probability. Using the fact that a particle chooses going up or down with an equal probability and it always moves forward,

$$\begin{aligned}\eta(\mathbf{x}-\mathbf{x}') &\equiv \langle \delta((\mathbf{x}-\mathbf{x}')-\Delta\mathbf{x})\rangle \\ &= \langle \delta((x-x')-lcos\theta_0)\delta((y-y')-l\xi sin\theta_0)\rangle \\ &= \delta(x-x'-lcos\theta_0)\frac{1}{2}\left[\delta(y-y'-lsin\theta_0)+\delta(y-y'+lsin\theta_0)\right]\end{aligned} \tag{2.22}$$

Therefore, we can rewrite the transition probability as following.

$$\left\langle \delta(\mathbf{x}-(\mathbf{x}'+\Delta\mathbf{x}))\overline{\delta(t-(t'+\Delta t))}\right\rangle = \eta(\mathbf{x}-\mathbf{x}')\psi(t-t') \tag{2.23}$$

Equation (2.23) is our key result: after white noise averaging and ensemble averaging, the spatial transition probability and time transition probability became independent, and each term is determined by spatial transition and transition time. The derived transition probability shows that our lattice fracture model with heterogeneous sorption can be represented exactly by uncorrelated Continuous Time Random Walk (CTRW) model [24, 29]. Using the property of a stationary field, we showed the spatial transition and transition time are independent after ensemble averaging which implies that the mean concentration can be effectively captured by CTRW. The equivalent CTRW model can be defined as following Langevin equations.

$$\begin{aligned}x_{N+1} &= x_N + lcos(\alpha)\\ y_{N+1} &= y_N + l\xi_N sin(\alpha)\\ t_{N+1} &= t_N + \frac{l}{v_N},\end{aligned} \tag{2.24}$$

where $p_{\xi_n} = \frac{1}{2}\delta(\xi_n+1)+\frac{1}{2}\delta(\xi_n-1)$ and v_N is sampled independently from $P(v)$.

By performing particle tracking simulation with the average model given in Equation (2.24), we can obtain the mean concentration. This is equivalent to solving Equation (2.17). Our CTRW average model can be verfied by comparing with the result in Section 2.2.3, where the mean concentration was obtained by Monte Carlo simulation. The contour plot shows that the mean concentration obtained from the CTRW model and the Monte Carlo simulation are identical as shown in Figure 2-7. Computing efficiency increased significantly by using the CTRW model. To obtain the mean concentration, we performed CTRW simulation for 5×10^4 particles, and for the Monte Carlo simulation, we performed particle tracking simulation for 10^4 realizations with 10^4 particles for each realization, which means we injected 10^8 particles in total.

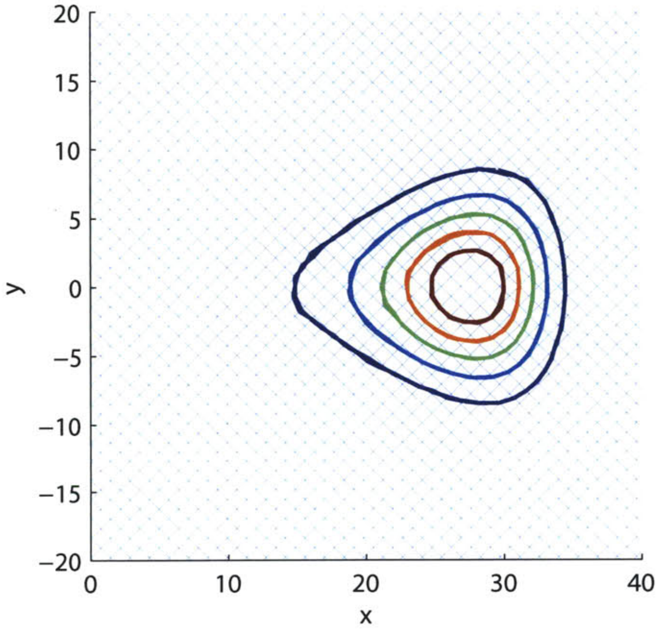

Figure 2-7: Comparison of the mean concentration obtained from Monte Carlo simulation over 10^4 realizations and uncorrelated CTRW Langevin equation. The two contour plots are almost identical which verifies that our CTRW model effectively captures the mean concentration.

2.2.5 Eulerian Formulation

The effective Langevin equations for the mean concentration describe transport in a particle level. Here, we derive dynamic Eulerian from of equations for the mean concentration. Using the developed transition probability in Section 2.2.4, we develop Eulerian formulation for the mean concentration.

$$P_N(\mathbf{x},t) = \int d\mathbf{x}' \int dt' \eta(\mathbf{x}-\mathbf{x}')\psi(t-t')P_{N-1}(\mathbf{x}',t') \tag{2.25}$$

Using Equation (2.25), we express $R(\mathbf{x},t)$ with the transition probability as following.

$$\begin{aligned}
\sum_{N=1}^{\infty} P_N(\mathbf{x},t) &= \int d\mathbf{x}' \int dt' \eta(\mathbf{x}-\mathbf{x}')\psi(t-t') \sum_{N=1}^{\infty} P_{N-1}(\mathbf{x}',t') \\
R(\mathbf{x},t) - P_0(\mathbf{x},t) &= \int d\mathbf{x}' \int dt' \eta(\mathbf{x}-\mathbf{x}')\psi(t-t')R(\mathbf{x}',t') \\
R(\mathbf{x},t) &= P_0(\mathbf{x},t) + \int d\mathbf{x}' \int dt' \eta(\mathbf{x}-\mathbf{x}')\psi(t-t')R(\mathbf{x}',t') \qquad (2.26)
\end{aligned}$$

Equation (2.17) and Equation (2.26) gives closed form of the mean concentration as following.

$$\begin{aligned}
\bar{c}(\mathbf{x},t) &= \int_0^t dt' \left[1 - \int_0^{t-t'} d\tau\psi(\tau)\right] R(\mathbf{x},t') \\
R(\mathbf{x},t) &= P_0(\mathbf{x},t) + \int d\mathbf{x}' \int dt' \eta(\mathbf{x}-\mathbf{x}')\psi(t-t')R(\mathbf{x}',t')
\end{aligned}$$

Now let's derive an Eulerian form of the governing equation for the mean concentration using Laplace transform and Taylor expansion. Laplace transform of Equation (2.17) can be written as,

$$\mathcal{L}(\bar{c}(\mathbf{x},t)) = \bar{c}^*(\mathbf{x},s) = \mathcal{L}\left\{\int_0^t dt' \int_{t-t'}^{\infty} \psi(\tau)d\tau R(\mathbf{x},t')\right\} = F^*(s)R^*(\mathbf{x},s) \tag{2.27}$$

In Equation (2.27) we substituted $\int_{t-t'}^{\infty} \psi(\tau)d\tau$ to $F(t-t')$.

$$F^*(s) = \mathcal{L}\left\{F(t)\right\} = \mathcal{L}\left\{\int_t^{\infty} d\tau\psi(\tau)\right\} \quad = \mathcal{L}\left\{1 - \int_0^t d\tau\psi(\tau)\right\} \\ = \frac{1-\psi^*(s)}{s} \tag{2.28}$$

By inserting Equation (2.28) into Equation (2.27), $R^*(\mathbf{x}, s)$ can be written as following.

$$R^*(\mathbf{x}, s) = \frac{s\bar{c}^*(\mathbf{x}, s)}{1-\psi^*(s)} \tag{2.29}$$

Now let's work on Equation (2.26). For the initial condition $P_0(\mathbf{x}, t)$, we take a point source at the origin which can be expressed as $P_0(\mathbf{x}, t) = \delta(\mathbf{x} - \underline{0})\delta(t-0)$. Laplace transform of Equation (2.26) using the initial condition can be written as following.

$$\begin{aligned} R^*(\mathbf{x}, s) \quad &= \delta(\mathbf{x}) + \mathcal{L}\left\{\int d\mathbf{x}'\eta(\mathbf{x}-\mathbf{x}')\int dt'\psi(t-t')R(\mathbf{x}', t')\right\} \\ &= \delta(\mathbf{x}) + \int d\mathbf{x}'\eta(\mathbf{x}-\mathbf{x}')\psi^*(s)R^*(\mathbf{x}', s) \\ &= \delta(\mathbf{x}) + \int d\mathbf{x}'\eta(\mathbf{x}')\psi^*(s)R^*(\mathbf{x}-\mathbf{x}', s) \end{aligned} \tag{2.30}$$

Combing with Equation (2.29),

$$\frac{s\bar{c}^*(\mathbf{x}, s)}{1-\psi^*(s)} = \delta(\mathbf{x}) + \int d\mathbf{x}'\eta(\mathbf{x}')\psi^*(s)\frac{s\bar{c}^*(\mathbf{x}-\mathbf{x}', s)}{1-\psi^*(s)} \tag{2.31}$$

Now let's further develop Equation (2.31).

$$s\bar{c}^*(\mathbf{x}, s) + \frac{s\psi^*(s)\bar{c}^*(\mathbf{x}, s)}{1-\psi^*(s)} = \delta(\mathbf{x}) + \int d\mathbf{x}'\eta(\mathbf{x}')\frac{s\psi^*(s)\bar{c}^*(\mathbf{x}-\mathbf{x}', s)}{1-\psi^*(s)} \tag{2.32}$$

From Equation (2.32),

$$s\bar{c}^*(\mathbf{x}, s) = \delta(\mathbf{x}) + \int d\mathbf{x}'\eta(\mathbf{x}')\frac{\psi^*(s)s}{1-\psi^*(s)}\left[\bar{c}^*(\mathbf{x}-\mathbf{x}', s) - \bar{c}^*(\mathbf{x}, s)\right] \tag{2.33}$$

Using Taylor expansion,

$$\bar{c}^*(\mathbf{x}-\mathbf{x}',s) \approx \bar{c}^*(\mathbf{x},s) - \mathbf{x}'\nabla\bar{c}^*(\mathbf{x},s) + \frac{1}{2}\nabla\mathbf{x}'\otimes\mathbf{x}'\nabla\bar{c}^*(\mathbf{x},s) + \cdots \tag{2.34}$$

Now let's insert Equation (2.34) into Equation (2.33)

$$s\bar{c}^*(\mathbf{x},s) \approx \delta(\mathbf{x}) - \left[\int d\mathbf{x}'\eta(\mathbf{x}')\mathbf{x}'\right]\frac{\psi^*(s)s}{1-\psi^*(s)}\nabla\bar{c}^*(\mathbf{x},s) + \nabla\left[\frac{1}{2}\int d\mathbf{x}'\mathbf{x}'\otimes\mathbf{x}'\eta(\mathbf{x}')\right]\nabla\bar{c}^*(\mathbf{x},s)\frac{\psi^*(s)s}{1-\psi^*(s)} \tag{2.35}$$

Now we define memory function($M^*(s)$) with a median transition time t_1 as,

$$M^*(s) = \frac{\psi^*(s)st_1}{1-\psi^*(s)} \tag{2.36}$$

and define $\bar{\mathbf{x}}$ and $\overline{\mathbf{x}^2}$ as,

$$\bar{\mathbf{x}} = \int d\mathbf{x}'\eta(\mathbf{x}')\mathbf{x}' \qquad\qquad \overline{\mathbf{x}^2} = \int d\mathbf{x}'\mathbf{x}'\otimes\mathbf{x}'\eta(\mathbf{x}') \tag{2.37}$$

The transition velocity is defined as $\mathbf{v} = \frac{\bar{\mathbf{x}}}{t_1}$, and the dispersion tensor is defined as $\mathbf{D} = \frac{\overline{\mathbf{x}^2}}{2t_1}$. Then we can write Equation (2.35) as,

$$s\bar{c}^*(\mathbf{x},s) = \delta(\mathbf{x}-\underline{0}) - \mathbf{v}\cdot[\nabla\bar{c}^*(\mathbf{x},s)]M^*(s) + \mathbf{D}:[\nabla\nabla\bar{c}^*(\mathbf{x},s)]M^*(s) \tag{2.38}$$

Now apply inverse Lapace transform to Equation (2.38) and we obtain Eulerian form of the governing equation for the mean concentration as following.

$$\frac{\partial}{\partial t}\bar{c}(\mathbf{x},t) = -\int_0^t M(t-t')\left[\mathbf{v}\cdot\nabla\bar{c}(\mathbf{x},t') - \mathbf{D}:\nabla\nabla\bar{c}(\mathbf{x},t')\right]dt' \tag{2.39}$$

We can obtain the analytical solution of the mean concentration by solving Equation (2.38). To solve Equation (2.38), we need to first calculate $\psi(t)$, $\bar{\mathbf{x}}$ and $\overline{\mathbf{x}^2}$. In our lattice fracture model, we showed that $\psi(t)$ can be derived from the particle velocity distribution. Now let's calculate $\bar{\mathbf{x}}$, $\overline{\mathbf{x}^2}$ for our lattice fracture model.

$$\begin{aligned}\bar{\mathbf{x}} &= \int d\mathbf{x}'\eta(\mathbf{x}')\mathbf{x}' \\ &= \int dx_1 \int dx_2 \eta(\mathbf{x}')\mathbf{x}' \\ &= (lcos\theta_0, 0)\end{aligned} \tag{2.40}$$

Now let's calculate for $\overline{\mathbf{x}^2}$.

$$\overline{\mathbf{x}^2} = \int d\mathbf{x}'\mathbf{x}' \otimes \mathbf{x}'\eta(\mathbf{x}') = \begin{pmatrix} \overline{x_1x_1} & \overline{x_1x_2} \\ \overline{x_2x_1} & \overline{x_2x_2} \end{pmatrix} \tag{2.41}$$

$$\overline{x_1x_1} = \int dx_1 \int dx_2 x_1^2 \left[\delta(x_1 - lcos\theta_0)\left(\frac{1}{2}\delta(x_2 - lsin\theta_0) + \frac{1}{2}\delta(x_2 + lsin\theta_0)\right)\right] = (lcos\theta_0)^2 \tag{2.42}$$

If we repeat the above calculation,

$$\begin{pmatrix} \overline{x_1x_1} & \overline{x_1x_2} \\ \overline{x_2x_1} & \overline{x_2x_2} \end{pmatrix} = \begin{pmatrix} (lcos\theta_0)^2 & 0 \\ 0 & (lsin\theta_0)^2 \end{pmatrix} \tag{2.43}$$

With $\eta(\mathbf{x}')$, $\psi(t)$, $\bar{\mathbf{x}}$ and $\overline{\mathbf{x}^2}$, we can fully determine coefficients in Equation (2.38) and can obtain analytical solution of the mean concentration using inverse Laplace. We use numerical code for the inverse Laplace. We verify our analytical solution by comparing with the mean concentration obtained from Monte Carlo simulation as shown in Figure 2-8.

The two contour plots in Figure 2-8 is almost identical, but we can notice slight difference in the plume front shape. This is caused by the second order approximation used in Taylor expansion and the numerical noise introduced in Laplace inversion. However, the difference is small and we can conclude that our effective equation gives correct solution. The developed CTRW model accurately captured the plume shape and, most importantly, the evolution are determined only by one parameter (β) which is the slope of the power law region. As a result, this model is also highly efficient for the parameter determination using inversion. In the real world, there is

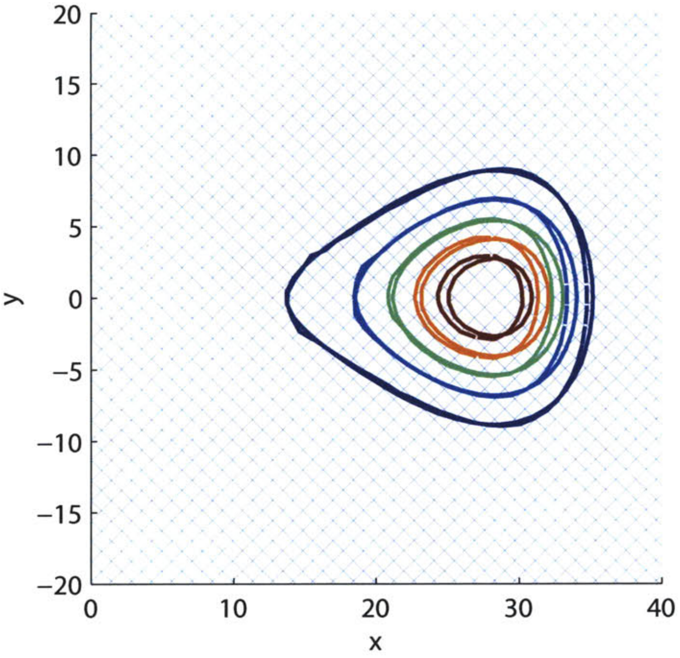

Figure 2-8: Comparison of the mean concentration from Monte Carlo simulation over 10^4 realizations and the analytical solution obtained by solving the Eulerian form of CTRW equation.

limited information and the model which has only one parameter is very attractive. However, this is only true when the velocity field is stationary and it follows power law distribution.

2.3 Transport Behavior

We now have an effective model for the mean concentration. Using this model, we can effectively study the transport behavior. Since the model has only one parameter which is β, we first check the sensitivity of the mean concentration with respect to β. Then we characterize the transport behavior with center of mass velocity and spreading of the mean concentration.

2.3.1 Sensitivity of Mean Concentration with respect to β

The effective macroscopic equation for mean concentration has essentially only one parameter β, and we check how this β affects the plume shape. $1+\beta$ is the slope of the power law region of the retardation factor probability density function. As shown in Figure 2-9, larger β has steeper slope in the power law region. Therefore, there is less probability of sampling large retardation factors compared to the smaller β. Inversely, small β indicates that there is relatively large probability of sampling extreme retardation factors which will cause anomalous transport.

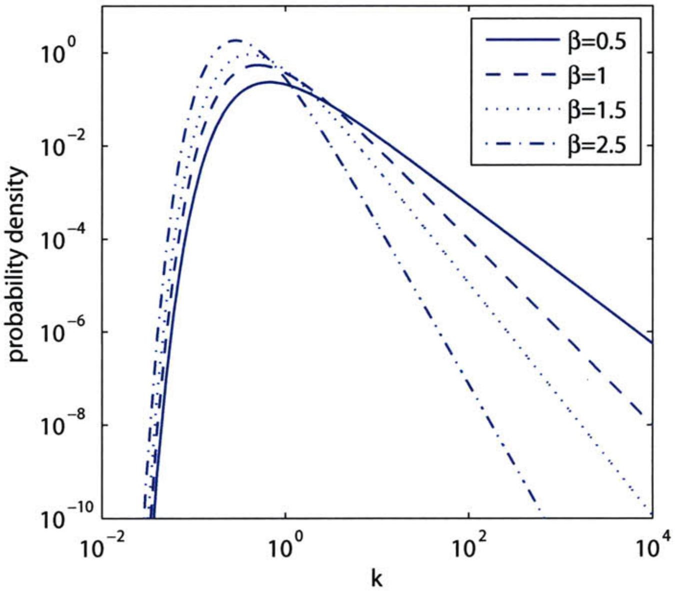

Figure 2-9: One-sided truncated power law distributions with four different βs. Large β indicates the range of sampling values is narrower compared to smaller β which has wide range of sampling values.

The impact of β value on the overall plume shape can be seen in Figure 2-10. It shows the mean concentration for four different β values at $t = 50$. The result shows significantly different plume shapes. For $\beta = .5$, most of the particles stay near the injection point. This is due to high probability of sampling large retardation factor. As β increases, the plume moves faster and the center of mass of the plume moves towards the front of the plume. For $\beta = 2.5$, there is very little particles that stuck behind and most of particles travel with similar x-directional velocity. This is due

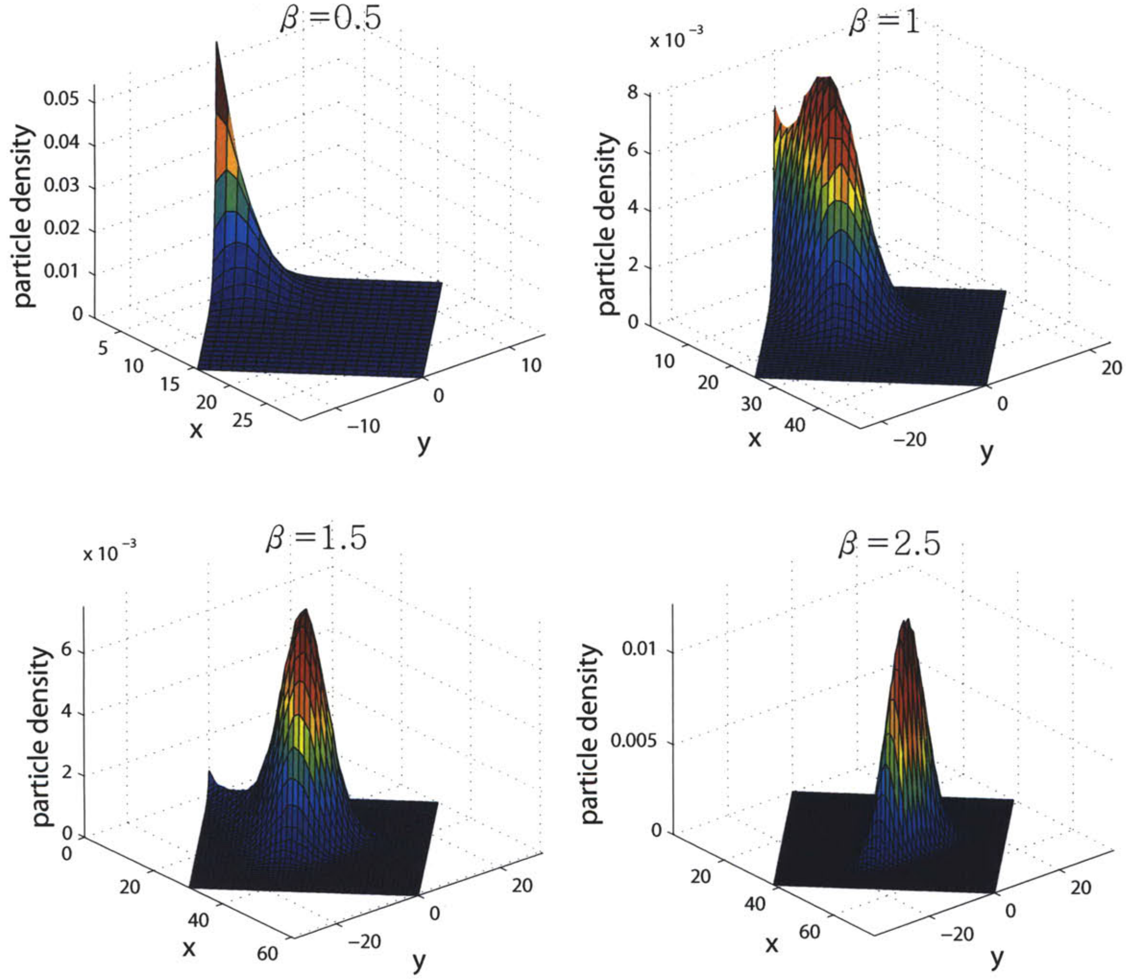

$\beta = 0.5$

$\beta = 1$

$\beta = 1.5$

$\beta = 2.5$

Figure 2-10: Mean concentration for four different values of β at $t = 50$. Shows the sensitivity of mean concentration with respect to β.

to large slope of power law region which cause narrow range of sampled retardation factor near small values.

2.3.2 Evolution of Spreading of the Mean Concentration

Now we characterize transport behavior with spreading of mean concetration. Figure 2-11 shows the evolution of spreading with respect to time, where spreading is defined as $\frac{1}{2}\left[m_{11}^{(2)}(t) - m_1^{(1)}(t)m_1^{(1)}(t)\right]$. $m_1^{(1)}(t)$ is the longitudinal first spatial moment and $m_{11}^{(2)}(t)$ is the longitudinal second spatial moment. The slope of the plot is corresponding to longitudinal dispersion coefficient. We can observe that $\beta = 1, 1.5$ has a similar trend and $\beta = 0.5, 2.5$ has a similar trend. This can explained by the plume shape in Figure 2-10. For $\beta = 1, 1.5$, it has intermediate β value. This intermidiate value causes strong tail. The plume center moves relatively fast, but some of the particles are left behind due to certain probability of sampling large retardation factor. Because particles are spreaded a lot, they have larger spatial second moment. For $\beta = 0.5, 2.5$, it has very small dispersion coefficient compared to $\beta = 1, 1.5$. For $\beta = 0.5$, most of particles stay near the injection point and for $\beta = 2.5$, most of particles moves with similar speed due to narrow sampling interval. Due to limited spreading, they have small dispersion coefficient. Change in slope or the slope different from 1 indicates that the transport through the lattice network is anomalous. For $\beta = 2.5$, the slope becomes 1, but for $\beta = 1, 1.5$, slope is not 1 which indicates that the transport is anomalous. For $\beta = 0.5$, we also observe the slope converging to 1 but this is by coincidence [16].

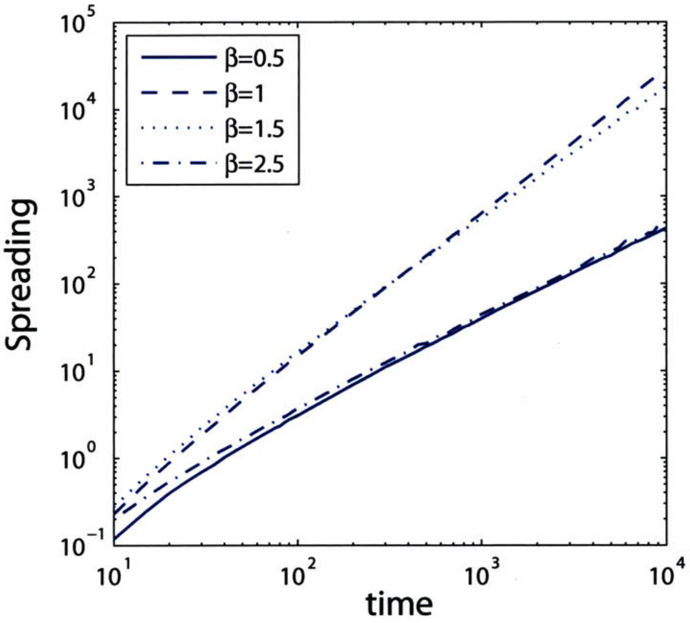

Figure 2-11: Evolution of spreading of mean concentration for four different values of β at $t = 50$. Shows that the transport is anomalous for $\beta < 2$.

Chapter 3

Development of the Analytical Model for the Concentration Variance

3.1 Variability of Concentration

Since the derived effective macroscopic equation gives the mean concentration, it is important to understand the variability of the concentration between realizations. As shown in Figure 2-5, the concentration field over each realization shows large variability. Figure 3-1 shows the probability density function of the concentration at the maximum mean concentration point. It has 10^4 data from Monte Carlo simulations. We can clearly see that it has large variance with highly skewed shape which again emphasizes the importance of understanding the variability between realizations. The standard deviation plot in Figure 3-1 explains variance of concentration at every node. It shows large variability near the injection point and the variability decreases with particle travel distance. This is due to the point injection initial condition and the power law velocity distribution. If particle transport velocity has extreme values near the injection point, it greatly impacts the overall plume shape since most of particle should travel through the fractures near the injection point. As particles travel and sample enough velocity statistics, the variance decreases. Combining the mean concentration and the variance of concentration, we can predict and understand transport behavior through the lattice fracture system. However, to obtain the information about the concentration variability, we had to run Monte Carlo simulation over 10^4 realizations which is numerically very expensive. Our goal in this chapter is to systematically and rigorously develop a concentration variance model which is numerically efficient.

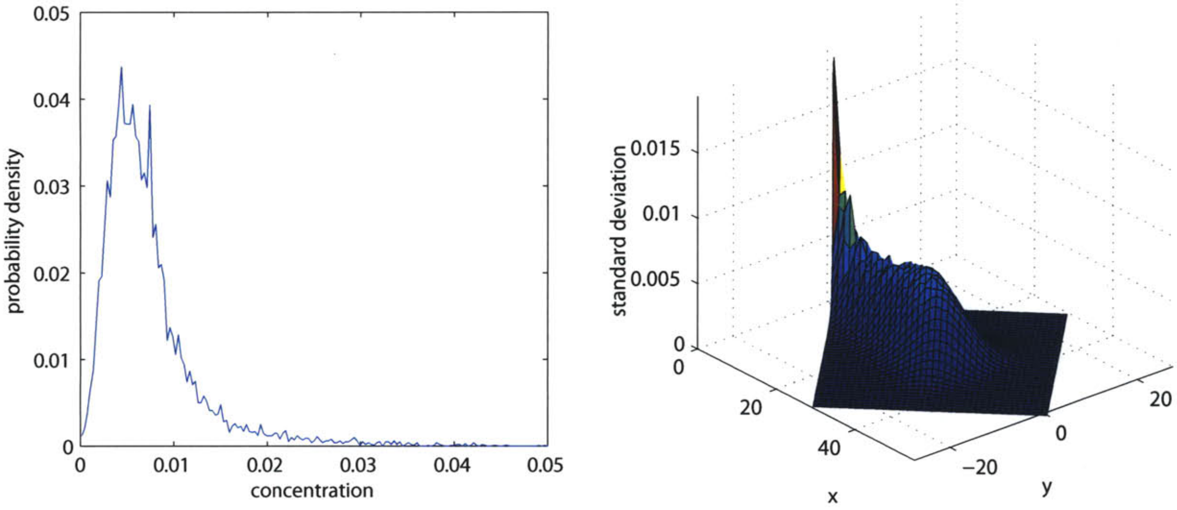

Figure 3-1: Concentration distribution at the maximum mean concentration point shows large variability between realizations. If we plot standard deviation at every point, we can obtain the figure on the right which shows that the varibaility is maximum near origin and decreases with travel distance.

3.2 Derivation of the Variance Model

Concentration variance can be written as following.

$$\begin{aligned} Var(c) &= \overline{(c(\mathbf{x},t) - \overline{c(\mathbf{x},t)})^2} \\ &= \overline{c(\mathbf{x},t)^2} - \overline{c(\mathbf{x},t)}^2 \end{aligned} \tag{3.1}$$

Since we have a model for the mean concentration $\overline{c(\mathbf{x},t)}$, what we need to know is the second moment of the concentration, $\overline{c(\mathbf{x},t)^2}$. We follow similar steps in Chapter 2 to work on the second moment of the concentration.

$$\begin{aligned}
\overline{c(\mathbf{x},t)^2} &= \overline{\left\langle \delta\left\{\mathbf{x}-\mathbf{x}[s(t)]\right\}\right\rangle^2} \\
&= \int ds \int ds' \overline{\left\langle \delta(\mathbf{x}-\mathbf{x}(s))\delta(s-s(t))\right\rangle \left\langle \delta(\mathbf{x}-\mathbf{x}(s'))\delta(s'-s(t))\right\rangle} \qquad (3.2)
\end{aligned}$$

We should perform the ensemble averaging prior to the noise averaging in order to utilize the stationarity of the velocity field. To perform ensemble averaging first, we have to make two seperate noise average into one. To this purpose, our key idea here is to think each term as two independent particles.

$$\begin{aligned}
\overline{c(\mathbf{x},t)^2} &= \int ds \int ds' \left\langle \overline{\delta(\mathbf{x}-\mathbf{x}^{(1)}(s))\delta(s-s^{(1)}(t))\delta(\mathbf{x}-\mathbf{x}^{(2)}(s'))\delta(s'-s^{(2)}(t))} \right\rangle \\
&= \int ds \int ds' \left\langle \delta(\mathbf{x}-\mathbf{x}^{(1)}(s))\delta(\mathbf{x}-\mathbf{x}^{(2)}(s'))\overline{\delta(s-s^{(1)}(t))\delta(s'-s^{(2)}(t))} \right\rangle \\
&= \sum_{N}\sum_{N'} \left\langle \delta(\mathbf{x}-\mathbf{x}_N^{(1)})\delta(\mathbf{x}-\mathbf{x}_{N'}^{(2)})\overline{\delta_{N,N_t^{(1)}}\delta_{N',N_t^{(2)}}} \right\rangle \qquad (3.3)
\end{aligned}$$

In our lattice fracture model, if the two particles arrived at the same location, N and N' are same. Otherwise, $\mathbf{x}_N^{(1)}$ and $\mathbf{x}_{N'}^{(2)}$ cannot be at the same location. Now let's further develop the time term using an indicator function (I).

$$\begin{aligned}
\overline{\delta_{N,N_t^{(1)}}\delta_{N',N_t^{(2)}}} &= \overline{I(t_N^{(1)} \le t < t_{N+1}^{(1)})I(t_N^{(2)} \le t < t_{N+1}^{(2)})} \\
&= \overline{I(0 \le t - t_N^{(1)} < t_{N+1}^{(1)} - t_N^{(1)})I(0 \le t - t_N^{(2)} < t_{N+1}^{(2)} - t_N^{(2)})} \\
&= \int_0^t dt' \int_0^t dt'' \overline{\delta(t'-t_N^{(1)})\delta(t''-t_N^{(2)})}\times \\
&\quad \overline{I\left(0 \le t - t' < \tau_N(\mathbf{x},\xi^{(1)})\right) I\left(0 \le t - t'' < \tau_N(\mathbf{x},\xi^{(2)})\right)}
\end{aligned}$$

Since t_N and τ_N are independent, we can break the ensemble averaging as following.

$$\begin{aligned}
\overline{\delta_{N,N_t^{(1)}}\delta_{N',N_t^{(2)}}} &= \int_0^t dt' \int_0^t dt'' \overline{\delta(t'-t_N^{(1)})\delta(t''-t_N^{(2)})}\times \qquad (3.4) \\
&\quad \overline{I\left(0 \le t - t' < \tau_N(\mathbf{x},\xi^{(1)})\right) I\left(0 \le t - t'' < \tau_N(\mathbf{x},\xi^{(2)})\right)} \qquad (3.5)
\end{aligned}$$

Now let's work on $\overline{I\left(0 \le t-t' < \tau_N(\mathbf{x},\xi^{(1)})\right) I\left(0 \le t-t'' < \tau_N(\mathbf{x},\xi^{(2)})\right)}$.

1) When two particles take the same path: $\xi^{(1)} = \xi^{(2)} = \xi$

$$\begin{aligned}
&\overline{I\left(0 \le t-t' < \tau_N(\mathbf{x},\xi)\right) I\left(0 \le t-t'' < \tau_N(\mathbf{x},\xi)\right)} \\
&= \int_0^\infty d\tau \psi(\tau) I\left(0 \le t-t' < \tau\right) I\left(0 \le t-t'' < \tau\right) \\
&= \int_{max(t-t',t-t'')}^\infty d\tau \psi(\tau)
\end{aligned} \tag{3.6}$$

Note that t' and t'' are different because they are the arrival times of two independent particles. When the two independent particles take the same link for the N^{th} jump, τ_N is same for the two particles.

2) When two particles take the different path: $\xi^{(1)} \ne \xi^{(2)}$

$$\begin{aligned}
&\overline{I\left(0 \le t-t' < \tau_N(\mathbf{x},\xi^{(1)})\right)}\ \overline{I\left(0 \le t-t'' < \tau_N(\mathbf{x},\xi^{(2)})\right)} \\
&= \int_0^\infty d\tau_1 \psi(\tau_1) I\left(0 \le t-t' < \tau_1\right) \int_0^\infty d\tau_2 \psi(\tau_2) I\left(0 \le t-t'' < \tau_2\right) \\
&= \int_{t-t'}^\infty d\tau_1 \psi(\tau_1) \int_{t-t''}^\infty d\tau_2 \psi(\tau_2)
\end{aligned} \tag{3.7}$$

Now we insert Equation (3.6) and Equation (3.7) into Equation (3.5).

$$\begin{aligned}
\overline{\delta_{NN_1(t)}\delta_{NN_2(t)}} &= \int_0^t dt' \int_0^t dt'' \overline{\delta(t'-t_N^1)\delta(t''-t_N^2)} \int_{max(t-t',t-t'')}^\infty d\tau \psi(\tau) \delta_{\xi^{(1)},\xi^{(2)}} + \\
&\int_0^t dt' \int_0^t dt'' \overline{\delta(t'-t_N^1)\delta(t''-t_N^2)} \int_{t-t'}^\infty d\tau_1 \psi(\tau_1) \int_{t-t''}^\infty d\tau_2 \psi(\tau_2) \delta_{\xi^{(1)},-\xi^{(2)}}
\end{aligned}$$

Therefore, the equation for the second moment of the concentration can be written as,

$$\begin{aligned}\overline{c(\mathbf{x},t)^2} = &\int_0^t dt' \int_0^t dt'' \sum_N \left\langle \delta(\mathbf{x}-\mathbf{x}_N^{(1)})\delta(\mathbf{x}-\mathbf{x}_N^{(2)})\overline{\delta(t'-t_N^{(1)})\delta(t''-t_N^{(2)})}\right\rangle \\ &\times \int_{\max(t-t',t-t'')}^{\infty} d\tau \psi(\tau)\langle \delta_{\xi^{(1)},\xi^{(2)}}\rangle \\ &+ \int_0^t dt' \int_0^t dt'' \sum_N \left\langle \delta(\mathbf{x}-\mathbf{x}_N^{(1)})\delta(\mathbf{x}-\mathbf{x}_N^{(2)})\overline{\delta(t'-t_N^{(1)})\delta(t''-t_N^{(2)})}\right\rangle \\ &\times \int_{t-t'}^{\infty} d\tau \psi(\tau) \int_{t-t''}^{\infty} d\tau \psi(\tau)\langle \delta_{\xi^{(1)},-\xi^{(2)}}\rangle . \end{aligned} \tag{3.8}$$

We now define the two-particle density after N steps as

$$P_N(\mathbf{x},t_1;\mathbf{y},t_2) = \left\langle \delta(\mathbf{x}-\mathbf{x}_N^{(1)})\delta(\mathbf{y}-\mathbf{x}_N^{(2)})\overline{\delta(t_1-t_N^{(1)})\delta(t_2-t_N^{(2)})}\right\rangle . \tag{3.9}$$

Thus, we can now write the second moment of concentration as,

$$\begin{aligned}\overline{c(\mathbf{x},t)^2} = &(a_+^2+a_-^2)\int_0^t dt' \int_0^t dt'' \sum_N P_N(\mathbf{x},t';\mathbf{x},t'') \int_{\max(t-t',t-t'')}^{\infty} d\tau \psi(\tau) \\ &+2a_+a_- \int_0^t dt' \int_0^t dt'' \sum_N P_N(\mathbf{x},t';\mathbf{x},t'') \int_{t-t'}^{\infty} d\tau \psi(\tau) \int_{t-t''}^{\infty} d\tau \psi(\tau) \end{aligned} \tag{3.10}$$

where a_+ is the probability that a particle goes upwards and a_- that it goes downwards. We express the two particle density $P_N(\mathbf{x},t_1;\mathbf{y},t_2)$ with a transition probability and $P_{N-1}(\mathbf{x},t_1;\mathbf{y},t_2)$, which is Chapman-Kolmogorov equation.

$$\begin{aligned}P_N(\mathbf{x},t_1;\mathbf{y},t_2) = &\int \mathrm{d}\mathbf{x}' \int_0^{t_1} \mathrm{d}t_1' \int \mathrm{d}\mathbf{y}' \int_0^{t_2} \mathrm{d}t_2' P_{N-1}(\mathbf{x}-\mathbf{x}',t_1-t_1';\mathbf{y}-\mathbf{y}',t_2-t_2') \\ &\times \left\langle \delta(\mathbf{x}'-\boldsymbol{\xi}_N^{(1)})\delta(\mathbf{y}'-\boldsymbol{\xi}_N^{(2)})\overline{\delta[t_1'-\tau_N(\mathbf{x}-\mathbf{x}',\eta_1)]\delta[t_2'-\tau_N(\mathbf{y}-\mathbf{y}',\eta_2)]}\right\rangle , \end{aligned} \tag{3.11}$$

where the increments $\boldsymbol{\xi}$ are defined by

$$\xi_x = l\cos(\alpha), \qquad \xi_y = \eta l \sin(\alpha), \tag{3.12}$$

The random variable η assumes the value 1 with probability a_+ and the value -1 with the probability a_-.

The two-particle transition length and time distribution is defined by

$$\psi_2(\mathbf{x}', t_1'; \mathbf{y}', t_2') = \\ \left\langle \delta(\mathbf{x}' - \boldsymbol{\xi}_N^{(1)})\delta(\mathbf{y}' - \boldsymbol{\xi}_N^{(2)})\overline{\delta[t_1' - \tau_N(\mathbf{x} - \mathbf{x}', \eta_1)]\delta[t_2' - \tau_N(\mathbf{y} - \mathbf{y}', \eta_2)]} \right\rangle . \tag{3.13}$$

For $\mathbf{x} \neq \mathbf{y}$ the time increments are independent and ensemble averaging and subsequent noise averaging gives

$$\psi_2(\mathbf{x}', t_1'; \mathbf{y}', t_2') = \psi_1(\mathbf{x}', t_1')\psi_1(\mathbf{y}', t_2'), \tag{3.14}$$

where $\psi_1(\mathbf{x}, t)$ is the one particle transition probability given by

$$\psi_1(\mathbf{x}, t) = \delta[x_1 - l\cos(\alpha)]\left\{a_+\delta[x_2 - l\sin(\alpha)] + a_-\delta[x_2 + l\sin(\alpha)]\right\}. \tag{3.15}$$

We are interested in the case that $\mathbf{x} = \mathbf{y}$. Let us consider now the ensemble average

$$\overline{\delta[t_1' - \tau_N(\mathbf{x} - \mathbf{x}', \eta_1)]\delta[t_2' - \tau_N(\mathbf{y} - \mathbf{y}', \eta_2)]}. \tag{3.16}$$

If $\eta_1 \neq \eta_2$ (which implies $\boldsymbol{\xi}_N^{(1)} \neq \boldsymbol{\xi}_N^{(2)}$) the average can be broken because $\tau_N(\mathbf{x} - \mathbf{x}', \eta_1)$ and $\tau_N(\mathbf{y} - \mathbf{y}', \eta_2)$ are independent,

$$\overline{\delta[t_1' - \tau_N(\mathbf{x} - \mathbf{x}', \eta_1)]}\ \ \overline{\delta[t_2' - \tau_N(\mathbf{y} - \mathbf{y}', \eta_2)]} = \psi(t_1')\psi(t_2'). \tag{3.17}$$

If $\eta_1 = \eta_2$, which together with $\mathbf{x} = \mathbf{y}$ implies also that $\mathbf{x} - \mathbf{x}' = \mathbf{y} - \mathbf{y}'$, the transition times are identical and we obtain

$$\overline{\delta[t_1' - \tau_N(\mathbf{x} - \mathbf{x}', \eta_1)]\delta[t_2' - \tau_N(\mathbf{y} - \mathbf{y}', \eta_1)]} = \psi(t_1')\delta(t_1' - t_2'). \tag{3.18}$$

Thus we can write Equation (3.11) for $\mathbf{x} = \mathbf{y}$ as

$$P_N(\mathbf{x}, t_1, \mathbf{x}, , t_2) = \int \mathrm{d}\mathbf{x}' \int_0^{t_1} \mathrm{d}t_1' \int \mathrm{d}\mathbf{y}' \int_0^{t_2} \mathrm{d}t_2' P_{N-1}(\mathbf{x} - \mathbf{x}', t_1 - t_1'; \mathbf{x} - \mathbf{y}', t_2 - t_2') \\ \times \psi_2(\mathbf{x}', t_1'; \mathbf{y}', t_2'), \tag{3.19}$$

where the two-particle transition length and time distribution density is now defined by

$$\psi_2(\mathbf{x}', t_1'; \mathbf{y}', t_2') = \left\langle \delta(\mathbf{x}' - \boldsymbol{\xi}_N^{(1)}) \delta(\mathbf{y}' - \boldsymbol{\xi}_N^{(2)}) \delta_{\eta_1, \eta_2} \right\rangle \psi(t_1') \delta(t_1' - t_2') \\ + \left\langle \delta(\mathbf{x}' - \boldsymbol{\xi}_N^{(1)}) \delta(\mathbf{y}' - \boldsymbol{\xi}_N^{(2)}) \delta_{\eta_1, -\eta_2} \right\rangle \psi(t_1') \psi(t_2'). \tag{3.20}$$

Using Equation (3.12) we can evaluate the average to obtain

$$\psi_2(\mathbf{x}', t_1'; \mathbf{y}', t_2') = \psi_g(\mathbf{x}', t_1') \delta(\mathbf{x}' - \mathbf{y}') \delta(t_1' - t_2') + \psi_u(\mathbf{x}', t_1'; t_2') \delta(x_1' - y_1') \delta(x_2' + y_2') \tag{3.21}$$

with

$$\psi_g(\mathbf{x}', t_1') = \delta[x_1' - l\cos(\theta_0)] \left\{ a_+^2 \delta[x_2' - l\sin(\theta_0)] + a_-^2 \delta[x_2' + l\sin(\theta_0)] \right\} \psi(t_1') \tag{3.22}$$

$$\psi_u(\mathbf{x}', t_1'; t_2') = \delta[x_1' - l\cos(\theta_0)] a_+ a_- \left\{ \delta[x_2' - l\sin(\theta_0)] + \delta[x_2' + l\sin(\theta_0)] \right\} \\ \times \psi(t_1') \psi(t_2'). \tag{3.23}$$

Inserting Equation (3.21) into Equation (3.19), we obtain

$$P_N(\mathbf{x}, t_1, \mathbf{x}, , t_2) = \int \mathrm{d}\mathbf{x}' \int_0^{t_1} \mathrm{d}t_1' P_{N-1}(\mathbf{x} - \mathbf{x}', t_1 - t_1'; \mathbf{x} - \mathbf{x}', t_1 - t_1') \psi_g(\mathbf{x}', t_1') \\ + \int \mathrm{d}\mathbf{x}' \int_0^{t_1} \mathrm{d}t_1' \int_0^{t_2} \mathrm{d}t_2' P_{N-1}(\mathbf{x} - \mathbf{x}', t_1 - t_1'; x_1 - x_1', x_2 + x_2', t_2 - t_2') \psi_u(\mathbf{x}', t_1', t_2'). \tag{3.24}$$

Equation (3.21) is our key result. It says that the second moment of concentration can be obtained by two-particle CTRW. This is equivalent to injecting a particle pair into many realizations. The two particles trasport through the lattice network independently, as long as they transport through different links. However, if the two particle happen to travel through same link, they should have identical transition time since we should think as the two particles are transporting through one realizaiton. If the two particles happen to arrive at same node at target time, we record it as success and if the two particle arrive at different positions, we record it as failure. The total number of injected particle pairs are used as normalization factor. The Langevin form of two-particle CTRW equation can be written as following.

$$x_1^{(N+1)} = x_1^{(N)} + l\cos(\theta_0), \quad x_2^{(N+1)} = x_2^{(N)} + \eta_1 l\sin(\theta_0), \quad t_1^{(N+1)} = t_1^{(N)} + \tau(x_2^{(N)}, \eta_1) \tag{3.25}$$

$$y_1^{(N+1)} = y_1^{(N)} + l\cos(\theta_0), \quad y_2^{(N+1)} = y_2^{(N)} + \eta_2 l\sin(\theta_0), \quad t_2^{(N+1)} = t_2^{(N)} + \tau(y_2^{(N)}, \eta_2). \tag{3.26}$$

We verify our two-particle CTRW model by comparing with the second moment obtained from Monte Carlo simulation. For two-particle CTRW simulation, we simulated until we obtain 10^5 success particle pairs. Figure 3-2 shows that the result obtained from Monte Carlo simulation and from two-particle CTRW simulation have similar shape. We can check that two-particle CTRW successfully captures the two peak shape. To compare the result more quantitatively, we plot the cut along x-axis. As we increase the number of success pairs, the cut converges to the result from Monte-Carlo simulation. Even with $1,000$ success pairs, we can capture the two peak behavior. Our two-particle CTRW model is numerically much more efficient than Monte-Carlo simulation.

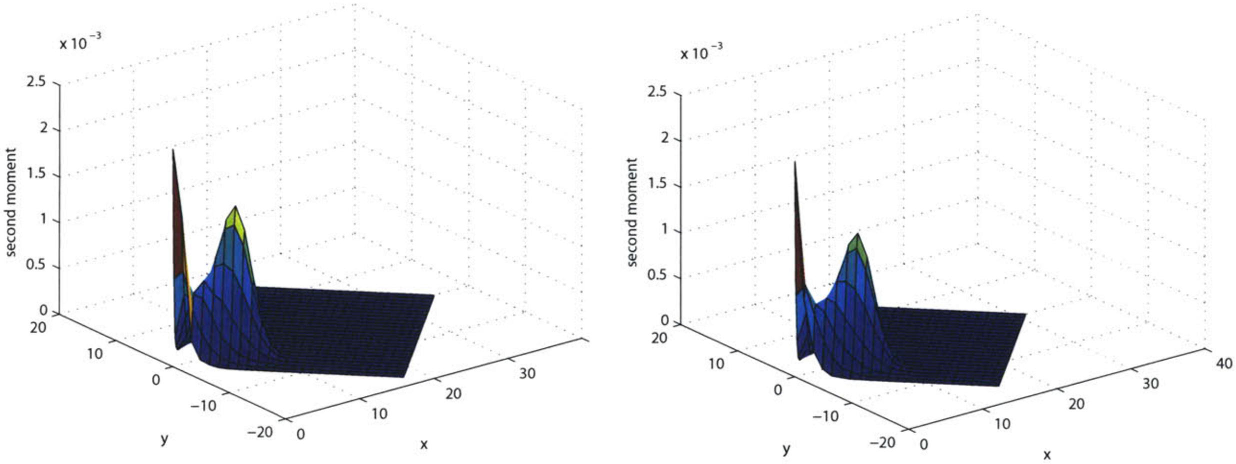

Figure 3-2: Comparison of second moment of concentration field from Monte Carlo simulation (left) and two-particle CTRW simulation (right).

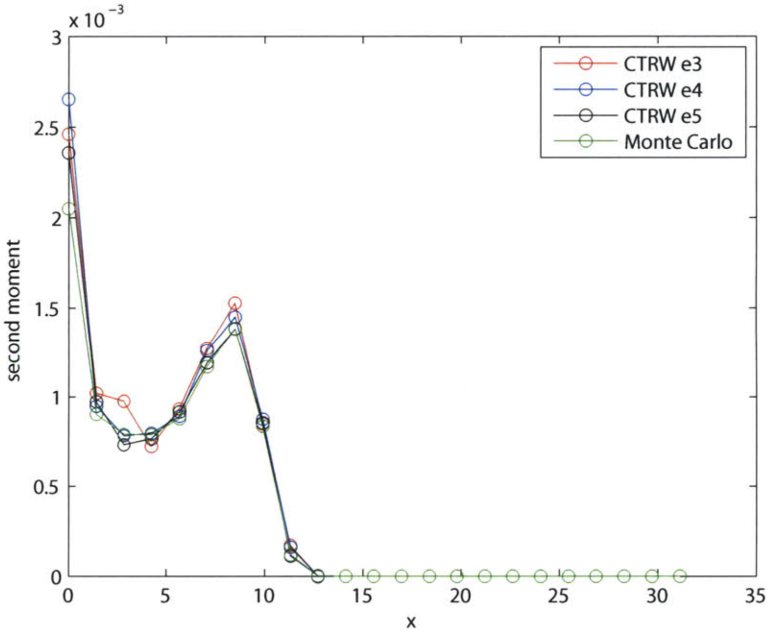

Figure 3-3: Comparison of second moment of concentration cuts along x-axis. With increasing the number of success particle pairs, it converges to the cut obtained from the Monte Carlo simulation.

3.3 Time Evolution of the Variability

Our variance model provides variability between realizations at fixed time. Another important information is time evolution of the variability. If variability decreases with transport time, it indicates that predictability increases with time. Figure 3-4 shows the time evolution of variability. If we plot time evolution of standard deviation of particle density at maximum particle density position, we observe power law decrease of variability. This indicates that the predictability is increasing with time. As particles travel through the lattice network, each particle sample transition time from each link. For large time, particles travel through many number of links and sample sufficient number of transition times. This explains why the variability decrease with time. At early time, each particles has large difference in sampled transition times, but the variability decrease as they sample enough transition times at large time.

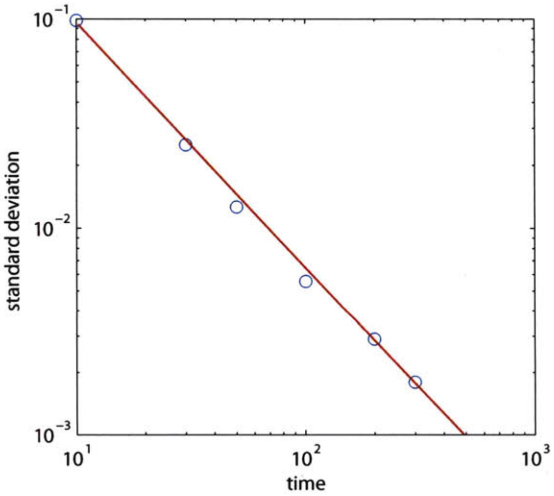

Figure 3-4: Time evolution of standard deviation of particle density at maximum particle density position

Chapter 4

Conclusions

We have developed an analytical model for the concentration mean and variance of particle transport in a lattice fracture network. The concentration mean was exactly and effectively captured by uncorrelated CTRW and the concentration variance by uncorrelated two particle CTRW. We verified our results by comparing the derived mean and variance behavior with direct numerical simulations of particle transport in single medium realizations and the corresponding ensemble average.

The significance of this work is that the macroscopic effective transport behavior has been derived directly from the local scale fracture description. It turns out that such macroscopic description takes the form of an uncorrelated CTRW. The description relies solely on the particle jumping time distribution, which depends —in our model— on a single parameter β. However, it is important to note that the CTRW model provides a description of the ensemble mean concentration, which is not an exact mean concentration for a specific realization. Therefore, information about variance between realizations is important for understanding predictability. Ensemble mean together with variance provides the essential information for quantification of effective transport in fractured media.

Most physical systems require correlated velocity field. In future work, we will try to generalize our model to incorporate correlated velocity fields. Based on some earlier work [12], we conjecture that the effective transport model may take the form of a correlated CTRW if the Lagrangian velocity is a spatial Markov process.

Bibliography

[1] R. Albert and A.-L. Barabási. Statistical mechanics of complex networks. *Rev. Mod. Phys.*, 74:47, 2002.

[2] D. Bächler and T. Kohl. Coupled thermal-hydraulic-chemical modelling of enhanced geothermal systems. *Geophys. J. Int.*, 161:533, 2005.

[3] S. Bachu. Sequestration of CO_2 in geological media: criteria and approach for site selection in response to climate change. *Energ. Convers. Manage.*, 41:953, 1999.

[4] G. I. Barenblatt, Iu. P. Zheltov, and I. N. Kochina. Basic concepts in the theory of seepage of homogeneous liquids in fissured rocks. *J. Appl. Math. Mech.*, 24:1286, 1960.

[5] J. Bear, C. F. Tsang, and G. de Marsily. *Flow and Contaminant Transport in Fractured Rock*. Academic, 1993.

[6] B. Berkowitz. Characterizing flow and transport in fractured geological media: A review. *Adv. Water Resour.*, 25:861, 2002.

[7] B. Berkowitz, A. Cortis, M. Dentz, and H. Scher. Modeling non-fickian transport in geological formations as a continuous time random walk. *Rev. Geophysics*, 44, 2006.

[8] B. Berkowitz, G. Kosakowski, G. Margolin, and H. Scher. Application of continuous time random walk theory to tracer test measurements in fractured and heterogeneous porous media. *Ground Water*, 39:593, 2001.

[9] B. Berkowitz and H. Scher. Anomalous transport in random fracture networks. *Phys. Rev. Lett.*, 79:4038, 1997.

[10] B. Berkowitz and H. Scher. Theory of anomalous chemical transport in random fracture networks. *Phys. Rev. E*, 57:5858, 1998.

[11] E. Bonnet, O. Bour, N. E. Odling, P. Davy, I. Main, P.Cowie, and B. Berkowitz. Scaling of fracture systems in geologic media. *Rev. Geophys.*, 39:347, 2001.

[12] T. Le Borgne, M. Dentz, and J. Carrera. Lagrangian statistical model for transport in highly heterogeneous velocity fields. *Phys. Rev. Lett.*, 101:090601, 2008.

[13] M. C. Cacas, E. Ledoux, and G. de Marsily. Modeling fracture flow with a stochastic discrete fracture network: Calibration and validation. 2. the transport model. *Water Resour. Res.*, 26:491, 1990.

[14] M. Dentz, D. Bolster, and T. Le Borgne. Concentration statistics for transport in random media. *Phys. Rev. E*, 80:010101, 2009.

[15] M. Dentz and A. Castro. Effective transport dynamics in porous media with heterogeneous retardation properties. *Geophys. Res. Lett.*, 36:L03403, 2009.

[16] M. Dentz, A. Cortis, H. Scher, and B. Berkowitz. Time behavior of solute transport in heterogeneous media: transition from anomalous to normal transport. *Adv. Water Resour.*, 27:155, 2004.

[17] W. S. Dershowitz and H. H. Einstein. Characterizing rock joint geometry with joint system models. *Rock Mech. Rock Eng.*, 21:21, 1988.

[18] G. D. Donato and M. J. Blunt. Streamline-based dual-porosity simulation of reactive transport and flow in fractured reservoirs. *Water Resour. Res.*, 40:W04203, 2004.

[19] H. H. Gerke and M. T. van Genuchten. A dual-porosity model for simulating the preferential flow of water and solutes in structured porous media. *Water Resour. Res.*, 29:305, 1993.

[20] B. Gong, M. Karimi-Fard, and L. J. Durlofsky. Upscaling discrete fracture characterizations to dual-porosity, dual-permeability models for efficient simulation of flow with strong gravitational effects. *SPE Journal*, 13:58, 2008.

[21] J. R. Gilman H. Kazemi and A. M. Elsharkawy. Analytical and numerical solution of oil recovery from fractured reservoirs with empirical transfer functions. *SPE J.*, 6:219–227, 1992.

[22] R. Juanes, J. Samper, and J. Molinero. A general and efficient formulation of fractures and boundary conditions in the finite element method. *Int. J. Numer. Meth. Eng.*, 54(12):1751–1774, 2002.

[23] M. Karimi-Fard, L. J. Durlofsky, and K. Aziz. An efficient discrete-fracture model applicable for general-purpose reservoir simulators. *SPE Journal*, 9:227, 2004.

[24] J. Klafter and R. Silbey. Derivation of the continuous time random walk equation. *Phys. Rev. Lett.*, 44:56, 1980.

[25] E.W. Montroll and G.H. Weiss. Random walks on lattice. 2. *J. Math. Phys.*, 6:167, 1965.

[26] L. Moreno and I. Neretnieks. Fluid flow and solute transport in a network of channels. *J. Contam. Hydrol.*, 14:163, 1993.

[27] S. P. Neuman. Multiscale relationships between fracture length, aperture, density and permeability. *Geophys. Res. Lett.*, 35:L22402, 2008.

[28] M. E. J. Newman. The structure and function of complex networks. *SIAM Review*, 45:167, 2003.

[29] H. Scher and M. Lax. Stochastic transport in a disordered solid. 1. theory. *Phys. Rev. B*, 7:4491–4502, 1973.

[30] H. Scher and E. W. Montroll. Anomalous transit-time dispersion in amorphous solids. *Phys. Rev. B*, 12:2455, 1975.

[31] N.F. Spycher, E.L. Sonnenthal, and J.A. Apps. Fluid flow and reactive transport around potential nuclear waste emplacement tunnels at yucca mountain, nevada. *J. Contam. Hydrol.*, 62:653, 2003.

[32] S. A. Tirén, P. Asklings, and S. Wänstedt. Geologic site characterization for deep nuclear waste dosposal in fractured rock based on 3d data visualization. *J. Eng. Geol.*, 52:319, 1999.

[33] J. E. Warren and P. J. Root. The behavior of naturally fractured reservoirs. *SPE Journal*, 228:245, 1963.